catalysts

MDPI

Article

Catalytic Activity of Nickel and Ruthenium–Nickel Catalysts Supported on SiO_2, ZrO_2, Al_2O_3, and $MgAl_2O_4$ in a Dry Reforming Process

Izabela Wysocka *, Jan Hupka and Andrzej Rogala

Department of Process Engineering and Chemical Technology, Faculty of Chemistry, Gdańsk University of Technology, 80-233 Gdańsk, Poland; jhupka@pg.edu.pl (J.H.); androgal@pg.edu.pl (A.R.)

* Correspondence: izabela.wysocka@pg.edu.pl; Tel.: +48-5834-72866

Received: 29 May 2019; Accepted: 11 June 2019; Published: 17 June 2019

Abstract: Dry reforming of methane (DRM) is an eco-friendly method of syngas production due to the utilization of two main greenhouse gases—methane and carbon dioxide. An industrial application of methane dry reforming requires the use of a catalyst with high activity, stability over a long time, and the ability to catalyze a reaction, leading to the needed a hydrogen/carbon monoxide ratio. Thus, the aim of the study was to investigate the effect of support and noble metal particles on catalytic activity, stability, and selectivity in the dry reforming process. Ni and Ni–Ru based catalysts were prepared via impregnation and precipitation methods on SiO_2, ZrO_2, Al_2O_3, and $MgAl_2O_4$ supports. The obtained catalysts were characterized using X-ray diffractometry (XRD), inductively coupled plasma optical emission spectrometry (ICP-OES), Brunauer–Emmett–Teller (BET) specific surface area, and elemental carbon-hydrogen-nitrogen-sulphur analysis (CHNS) techniques. The catalytic activity was investigated in the carbon dioxide reforming of a methane process at 800 °C. Catalysts supported on commercial Al_2O_3 and spinel $MgAl_2O_4$ exhibited the highest activity and stability under DRM conditions. The obtained results clearly indicate that differences in catalytic activity result from the dispersion, size of an active metal (AM), and interactions of the AM with the support. It was also found that the addition of ruthenium particles enhanced the methane conversion and shifted the H_2/CO ratio to lower values.

Keywords: dry reforming; nickel; ruthenium; the effect of support; syngas

1. Introduction

Synthetic gas is one of the most important substrates in the chemical industry. It serves as a substrate in the synthesis of various chemicals, such as methanol, liquid synthetic motor fuels, naphtha, diesel, methane, and dimethyl ether [1,2]. Syngas is mainly produced via methane reforming and biomass gasification. Production technology and further applications of syngas strongly depend on the hydrogen to carbon monoxide molar ratio [1–4]. Among the reforming techniques, dry reforming (DRM) of methane has attracted much attention due to the utilization of two abundantly available greenhouse gases (methane and carbon dioxide) and a final H_2/CO ratio that is close to unity [5,6]. Additionally, dry reforming requires only atmospheric pressure, however, the production of syngas via dry reforming at elevated pressures may be more practical because compression after the synthesis may lead to technical problems due to the high content of carbon monoxide [7,8].

Dry reforming is seen as an industrially immature process. A major limitation is the lack of an appropriate catalyst that exhibits high stability over a long time and high resistance to sintering and carbon deposition [1,9]. The most widely used and described catalysts are based on Ni particles. In comparison to noble metal catalysts, Ni catalysts are cheaper and exhibit similar or even higher

activity. Despite high catalytic activity, catalysts based on nickel suffer from the sintering of Ni particles and coke formation. Carbon deposits lastingly deactivate the catalysts and further block the gas flow through a reactor. The sintering of nickel particles leads to the formation of particle aggregates, decreased activity, and enhanced carbon deposition. It was found that carbon deposits possess a greater tendency to deposit on Ni particles of a larger size [1,6,9–11].

There are many strategies dedicated to prolonging catalysts' efficiency and life-time. One of the most popular strategies is to diminish the nickel particle size. However, high temperatures applied during the DRM process cause the sintering and aggregation of Ni particles. An enhancement of Ni particles' dispersion and stability may be provided via the deposition of noble metal nanoparticles. Noble metal particles, such as platinum, gold, rhodium, and ruthenium, may enhance the dispersion of nickel particles and inhibit carbon deposition [10,12–15]. Arora et al. [1] typed the properties of noble metals, such as a good dispersion ability in the form of nanoscale particles that promote the dissociative adsorption of hydrogen and oxygen, and the exposure of d-subshell electrons as the main features responsible for the high activity and coke resistance. Ruthenium nanoparticles were also successfully used for tuning the hydrogen/carbon monoxide molar ratio [16]. The coupling of nickel particles into alloys or spinel structures with other non-noble elements, such as Co [17,18], Cr [18], Mn [18–20], Ce [19,21], Fe [22,23], Zr [24], and Al [20,24], and alkali metals, such as Mg [25,26], K [27,28], and Na [29], was also reported as an effective approach to extend catalyst activity and reduce carbon formation [18,30]. Another technique used to preserve the small size of nickel particles is an application of a support that strongly interacts with the active metal. It was previously reported that the strong interaction and high binding energies of the active metal and support allow small particles to be obtained during the synthesis of the catalyst [31]. Moreover, strong interaction between an active metals and a support may also minimize aggregation due to Ni being retained. Zhang et al. [32] investigated the effect of TiO_2, ZrO_2, SiO_2, Al_2O_3, and MgO supports on the catalytic activity of nickel catalysts in the DRM process. They found that a strong interaction between NiO particles and MgO and Al_2O_3 resulted in a superior catalytic performance, high dispersion, and stabilization of NiO species. It was also previously reported in the literature that the introduction of an active metal into uniform mesoporous channels of supports or encapsulation into sandwich or core-shell structures may efficiently reduce the mobility of Ni particles known as the "anchoring effect", therefore, providing large dispersion, a metal particle size, and uniform distribution. Incorporated nickel particles in the channels or sandwich-like structures are protected against sintering under drastic dry reforming conditions [17,21,33,34]. The nature of the support may also have a significant impact on the catalytic activity. The basic character of MgO promotes the adsorption of carbon monoxide and carbon gasification. Ferreira-Aparicio et al. [35] investigated the role of a support (SiO_2 and Al_2O_3) on the catalytic activity of ruthenium catalysts during the dry reforming process. They found that for a silica support, both carbon dioxide and methane are activated on Ru particles, whereas for the Al_2O_3 support a bifunction mechanism was proposed, in which surface hydroxyl groups play a main role in the catalyst's resistance to deactivation. Frontera et al. [36] found that the structure of the support also determines the catalytic activity by influencing the nickel particles' size. They examined silica supports of different structures: Silicate-1, MCM-41, and TIQ-6. They found that the higher the level of defects and heterogeneity, the higher dispersion of nickel particles and catalytic activity.

A majority of articles present in the literature investigated the effect of the support for single-metal catalysts, the effect of the active metal particles' size, coupling with other non-noble metals, and an evaluation of the process parameters on the catalytic activity. To the best of our knowledge, there are few articles regarding the modification of selected supports with both ruthenium and nickel particles. In this regard, in our study, results of the catalytic activity of nickel and nickel-ruthenium catalysts supported on $MgAl_2O_4$, Al_2O_3, SiO_2, and ZrO_2 are presented.

2. Results

2.1. Catalyst Characterization

Sample labelling, final metal loadings, values of average crystalline anatase size, phase composition, and BET surface areas are presented in Table 1. Theoretical metal contents equaled 7 and 1 wt.% for nickel and ruthenium, respectively. ICP-OES analysis confirmed that the final metal loadings were close to theoretical values. The nickel content ranged from 6.02 ± 0.30 wt.% to 8.40 ± 0.47 wt.% for Ni/SiO_2 and Ni/ZrO_2, respectively. The content of ruthenium particles fluctuated from 0.56 ± 0.01 wt.% to 0.81 ± 0.07 wt.% for $Ru\text{-}Ni/Al_2O_3$ and $Ru\text{-}Ni/ZrO_2$, respectively.

Table 1. Characteristics of the physicochemical properties of Ni and Ni–Ru catalysts.

Catalyst	Metal Content (wt.%)		Surface Area S_{BET} (m^2 g^{-1})	Phase Composition					
				Support		Catalytically Active Phase			
						Nickel(II) Oxide		Ruthenium(IV) Oxide	
	Ni	Ru		d (nm)	S–Q (wt.%)	d (nm)	S–Q (wt.%)	d (nm)	S–Q (wt.%)
SiO_2	-	-	300	1	100	-	-	-	-
Ni/SiO_2	6.02 ± 0.30	-	391	1	100	n.d.	-	-	-
$Ru\text{-}Ni/SiO_2$	6.93 ± 0.35	0.75 ± 0.04	151	1	76 ± 8	19	19 ± 5	8	5 ± 5
Al_2O_3	-	-	7	41	100	-	-	-	-
Ni/Al_2O_3	8.00 ± 0.40	-	6	41	95 ± 3	22	5 ± 1	-	-
$Ru\text{-}Ni/Al_2O_3$	8.18 ± 0.41	0.66 ± 0.02	6	41	95 ± 4	21	5 ± 1	n.d.	-
$MgAl_2O_4$	-	-	145	3	100	-	-	-	-
$Ni/MgAl_2O_4$	6.74 ± 0.24	-	98	3	100	n.d.	-	-	-
$Ru\text{-}Ni/MgAl_2O_4$	6.78 ± 0.23	0.56 ± 0.01	169	3	99 ± 9	n.d.	-	32	1 ± 2
ZrO_2	-	-	30	15	100	-	-	-	-
Ni/ZrO_2	8.40 ± 0.47	-	23	17	94 ± 5	22	6 ± 5	-	-
$Ru\text{-}Ni/ZrO_2$	7.40 ± 0.47	0.81 ± 0.07	23	15	95 ± 7	19	5 ± 3	n.d.	n.d.

The surface area determined using the Brunauer–Emmett–Teller method ranged from 391 to 6 m^2 g^{-1} for Ni/SiO_2 and both Ni/Al_2O_3 and $Ru\text{-}Ni/Al_2O_3$, respectively. For silica supported catalysts, the BET surface area increased due to the high dispersion of nickel particles from 300 to 391 m^2 g^{-1} for SiO_2 and Ni/SiO_2, respectively. The deposition of ruthenium oxide particles resulted in a two-fold reduction of S_{BET} in comparison to Ni/SiO_2. In the case of alumina-supported catalysts, the deposition of nickel oxide and ruthenium oxide particles did not influence the S_{BET}-values for Al_2O_3, Ni/Al_2O_3, and $Ru\text{-}Ni/Al_2O_3$, which were almost the same. Values of the BET surface area for spinel-supported catalysts varied from 98 m^2 g^{-1} for $Ni/MgAl_2O_4$ to 169 m^2 g^{-1} for $Ru\text{-}Ni/MgAl_2O_4$. Catalysts supported on zirconium(IV) oxide were characterized by a similar BET surface area and ranged from 23 to 30 m^2 g^{-1} for Ni/ZrO_2 and ZrO_2, respectively.

Results of the XRD measurements are presented in Figure 1a–d and Table 1. The letter, S, refers to the reflections assigned to SiO_2 and N-NiO, R represents RuO_2, A refers to Al_2O_3, M to $MgAl_2O_4$, and Z to ZrO_2.

Figure 1a represents the diffraction spectra of SiO_2-supported catalysts. For SiO_2 and Ni/SiO_2 samples, the only reflection attributed silica were observed. A broad peak with a maximum at 23.5° indicates the presence of amorphous silica [32,37]. In the case of the $Ni\text{-}SiO_2$ catalyst, the absence of reflections assigned to nickel oxide may indicate a high dispersion and small size of the NiO particles. As has already been reported in the literature, the lack of peaks attributed to particular components of a sample may be a result of high dispersion, low content, or small sizes of crystals [16,32,34]. The presence of nickel element was confirmed using inductively coupled plasma atomic emission spectroscopy nalysis. For $Ru\text{-}Ni/SiO_2$, peaks attributed to NiO and RuO_2 were also observed. The observed reflections at 2θ equal to 28.01°, 35.18°, and 54.32° correspond to the RuO_2 crystallographic planes [1 1 0], [1 0 1], and [2 2 1], respectively [13]. Peaks attributed to NiO particles at 2θ 37.12°, 43.15°, 62.75°, 75.16°, and 79.32° refer to [1 1 1], [2 0 0], [2 2 0], [3 1 1], and [2 2 2], respectively [13,18,32].

The average crystalline size of RuO_2 and NiO equaled 8 and 19 nm. The content of RuO_2 and NiO crystals calculated using the Rietveld method equaled 19 ± 5 wt.% and 5 ± 5 wt.%, respectively.

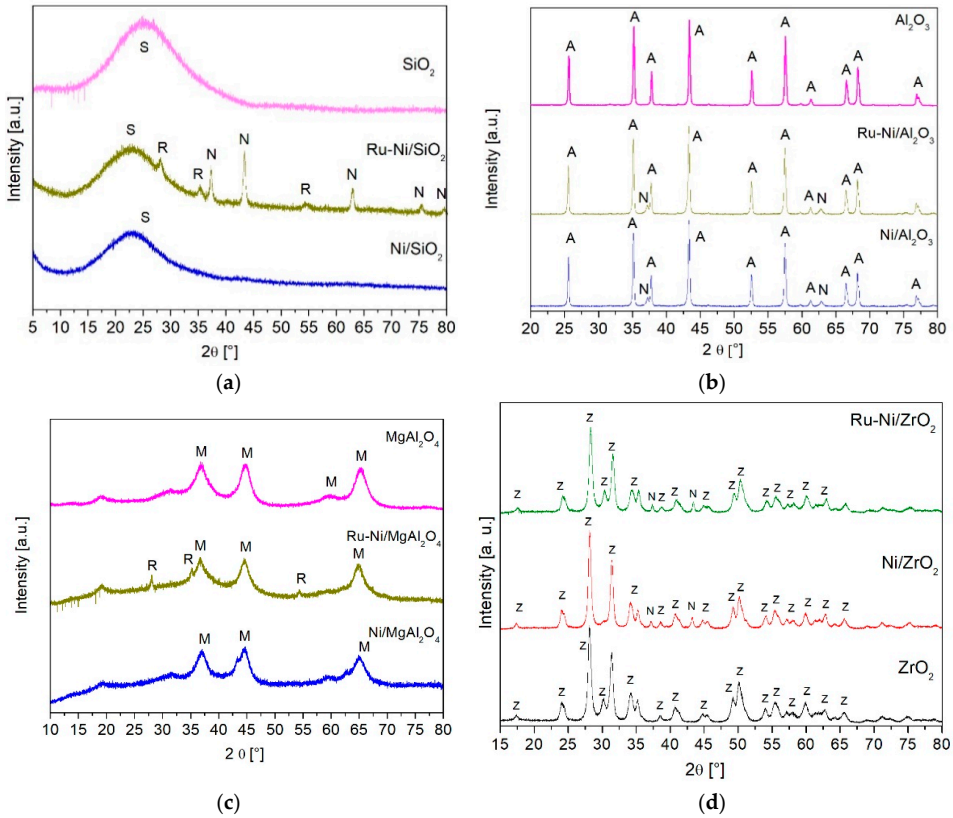

Figure 1. XRD patterns of nickel and ruthenium–nickel catalysts supported on (**a**) SiO_2, (**b**) Al_2O_3, (**c**) $MgAl_2O_4$, and (**d**) ZrO_2.

Figure 1b presents the diffraction spectra of the alumina-supported catalysts. In the case of aluminum(III) oxide, reflections at an angle of 2θ equal to 25.57°, 35.14°, 37.77°, 43.35°, 52.53°, 57.48°, 57.7°, 61.28°, 66.51°, 68.19°, 70.32°, 76.85°, and 77.20° correspond to the crystallographic systems [0 1 2], [1 0 4], [1 1 0], [1 1 3], [0 2 4], [1 1 6], [2 1 1], [1 2 2], [2 1 4], [3 0 0], [1 2 5], [1 0 10], and [1 1 9], respectively. For nickel(II) oxide, the observed reflections at 2θ angles of 37.22° and 62.81° correspond to crystalline structures [1 1 1] and [2 2 0]. The average crystalline size of alumina equaled 41 nm for all catalysts. The size of the NiO crystals for Ni-Al_2O_3 and Ru-Ni/Al_2O_3 was similar and reached 21 and 22 nm, respectively. The content of NiO was similar to theoretical contents and equaled 5 ± 1 wt.%. Any reflections attributed to ruthenium(IV) oxide were observed which may indicate a high dispersion and small sizes of the RuO_2 particles. The presence of the ruthenium element was conformed using ICP analysis.

In Figure 1c, XRD patterns of $MgAl_2O_4$ spinel catalysts are presented. Reflections in the 2θ range of 10 to 80° at 2 θ = 19.13°, 36.50°, 44.48°, and 64.98° are well-indexed as crystalline $MgAl_2O_4$ crystalline planes [1 1 1], [3 1 1], [4 0 0], and [4 4 0], respectively [38,39]. The average crystallite size of the magnesium–aluminum spinel was about 3 nm. Peaks attributed to active metals were observed only for RuO_2 at 2θ 28.01°, 35.32°, and 54.35° and corresponded to the [1 1 0], [1 0 1], and [2 1 1] planes, respectively. It was previously reported that during the synthesis of nickel–spinel catalysts other compounds, such as MgO, Al_2O_3, and $NiAl_2O_4$, may be formed [39–41]. However, XRD analysis did not show the presence of other species, thus they were not formed during the preparation.

XRD patterns for the last group of catalysts—supported on ZrO_2—are presented in Figure 1d. The average crystalline size of the bare support equaled 15 nm for Ni/ZrO_2 17 nm and for Ru-Ni/ZrO_2, 15 nm. Peaks attributed to NiO were observed for both Ni/ZrO_2 and Ru-Ni Ni/ZrO_2. Sizes of crystallites calculated based on the Scherrer equation were similar for the samples and equaled 22

and 19 nm. No reflexions for the ruthenium species were observed, indicating small sizes and a high distribution [41]. The presence of the ruthenium element was confirmed using ICP analysis.

2.2. Catalytic Activity

2.2.1. Nickel Catalysts

Results of the catalytic activity tests of nickel catalysts supported on SiO_2, ZrO_2, Al_2O_3, and $MgAl_2O_4$ are presented in Figure 2a–c. In the graphs, the results for supports are not included due to their negligible catalytic activity. The highest conversion for methane and carbon dioxide was obtained for Ni/Al_2O_3 and $Ni/MgAl_2O_4$ catalysts. The conversion level of CH_4 for the Ni/Al_2O_3 after two hours of the process remained stable at around 95%. In the case of the catalyst deposited on the magnesium–alumina spinel support, the efficiency of the methane conversion after 30 min of the process started decreasing to a final level of 80%. The consumption of carbon dioxide for both catalysts was observed at a steady level of 85%. Significant differences were observed in the generation of hydrogen and carbon monoxide. The highest molar ratio of hydrogen to carbon(II) oxide was close to what was also observed for the catalysts, Ni/Al_2O_3 and $Ni/MgAl_2O_4$. Throughout the catalytic process, the n_{H_2}/n_{CO} ratio for Ni/Al_2O_3 ranged from 0.95 to 1.0, whereas for $Ni/MgAl_2O_4$, it was constant at 0.9.

The lowest activity was recorded for the catalyst obtained on a silica support. Throughout the process, the methane conversion reached 37%, while the carbon dioxide conversion level was about 50%. The Ni/ZrO_2 catalyst was characterized by an initial higher activity compared to Ni/SiO_2; however, after one hour, a 20% drop in methane conversion was observed. The decrease in the activity of the catalyst deposited on the support of zirconium(IV) oxide is probably a result of carbon deposits' formation on the catalyst surface, causing the blocking of active sites and throttling the flow of gases through the bed. The final molar ratio of n_{H_2}/n_{CO} for Ni/ZrO_2 was dropped from 0.75 to 0.55.

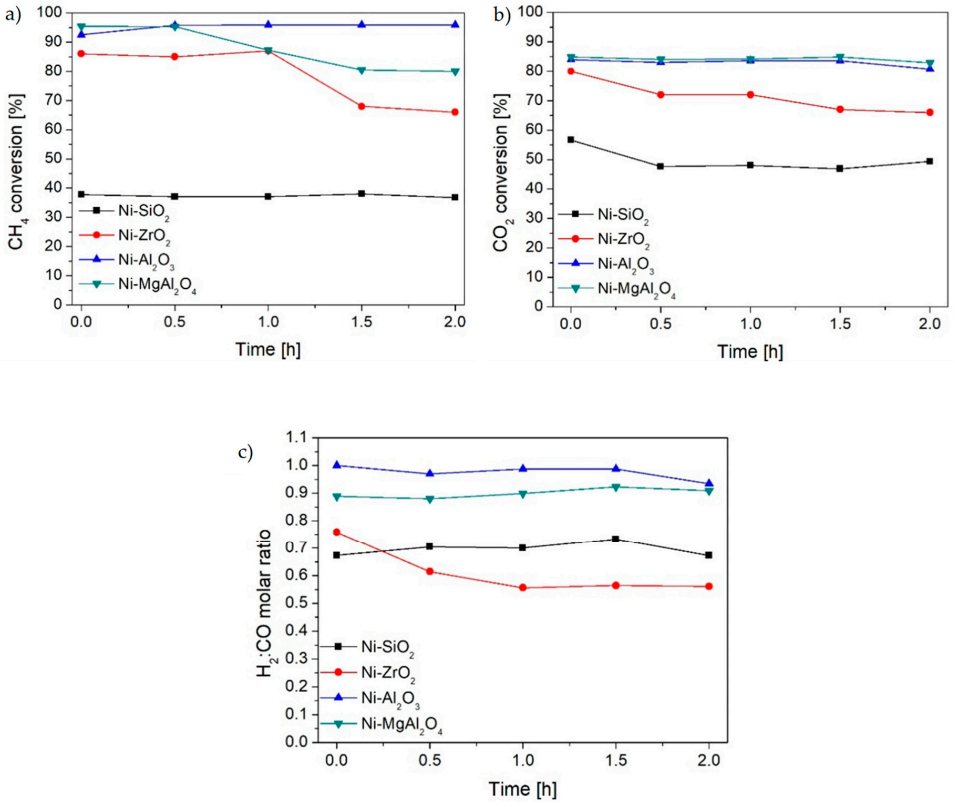

Figure 2. (**a**) Methane conversion, (**b**) carbon dioxide conversion, and (**c**) H_2/CO molar ratio for nickel catalysts.

2.2.2. Ruthenium–Nickel Catalysts

In Figure 3a–c, the results of tests on the activity of ruthenium–nickel catalysts are presented. The highest activity was observed for the Ru-Ni/Al_2O_3 catalyst. In comparison to Ni/Al_2O_3, an increase in activity due to the deposition of small ruthenium particles was observed. The conversion of methane remained stable—100% during the entire process—while the conversion of carbon dioxide ranged from 90% at the beginning to 71% after two hours. The molar ratios of hydrogen to carbon monoxide were lower in comparison to the catalysts containing only nickel particles. At the beginning of the process, it was 0.75 and it decreased during the process to 0.6. In the case of the Ru-Ni/$MgAl_2O_4$ catalyst, the complete conversion of methane was also observed. The conversion of carbon(IV) oxide ranged from 85% to 75% at the beginning and after 2 h of the process, respectively. The molar ratio of hydrogen/carbon monoxide was also slightly reduced from 0.67 to 0.61. The results obtained for the generation of CO and H_2 are similar to the results obtained for Ni/$MgAl_2O_4$; however, the molar ratio of H_2:CO was lower. The lack of catalytic activity enhancement is probably assigned to the deposition of large RuO_2 particles. The lowest catalytic activity among the tested catalysts was observed for the Ru-Ni/SiO_2 catalyst. The deposition of small ruthenium(IV) oxide particles on the silica surface resulted in an increase in the catalytic activity compared to Ni-SiO_2. The conversion of methane increased from 37% to 60% to 64%. The degree of conversion of carbon(IV) oxide, however, remained at a similar level, around 50%. The H_2:CO molar ratio was noted to be in the range of 0.70 to 0.53.

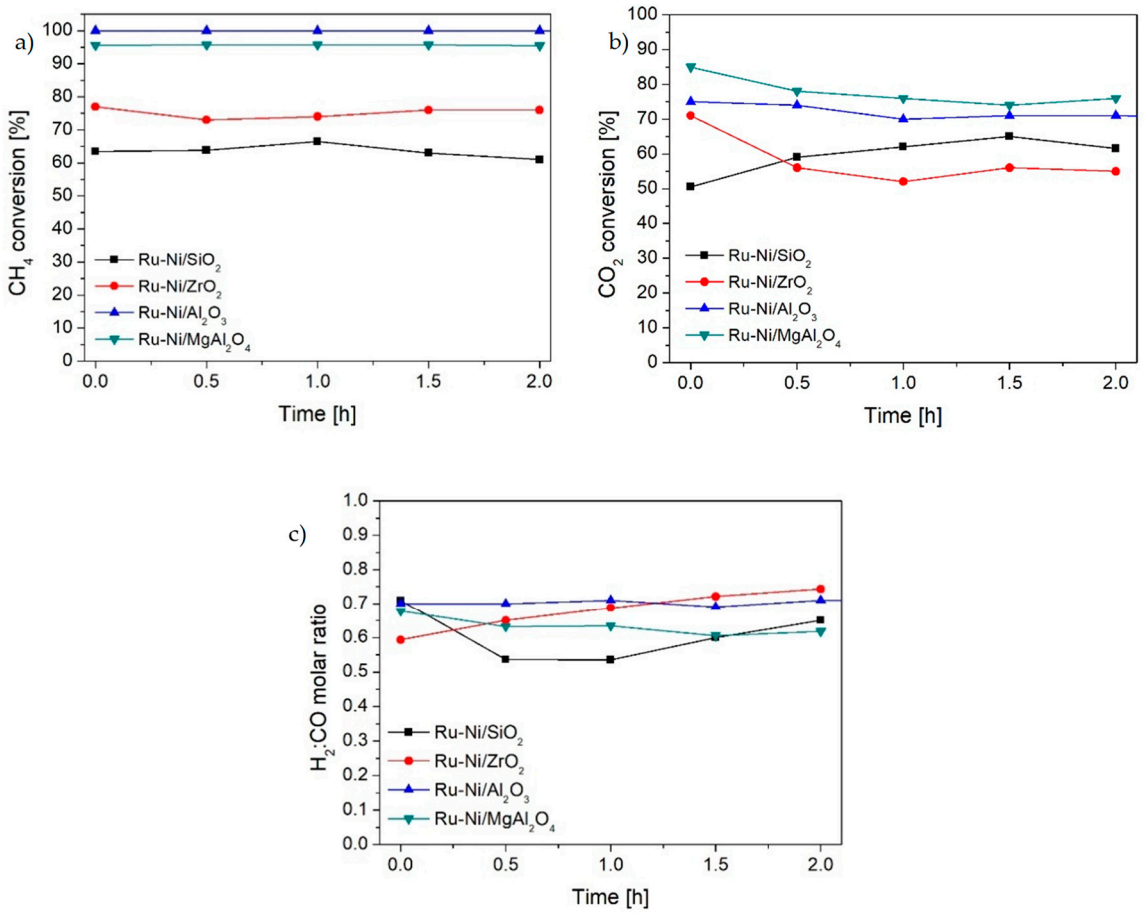

Figure 3. (**a**) Methane conversion, (**b**) carbon dioxide conversion, and (**c**) H_2/CO molar ratio for ruthenium–nickel catalysts.

Among the tested ruthenium–nickel catalysts, Ru-Ni/Al_2O_3 was characterized by one of the highest activity and stability during 2 h test, thus its stability was examined during the 6 h test. Figure 4a,b show the results of the analysis. The methane conversion rate remained constant at 98%

to 100% for 6 h of the process. The degree of CO_2 conversion during the process was also constant; after six hours the conversion rate reached 75%. The molar ratio of H_2:CO decreased from 0.75 to 0.55 at the beginning and after 6 h of the process, respectively.

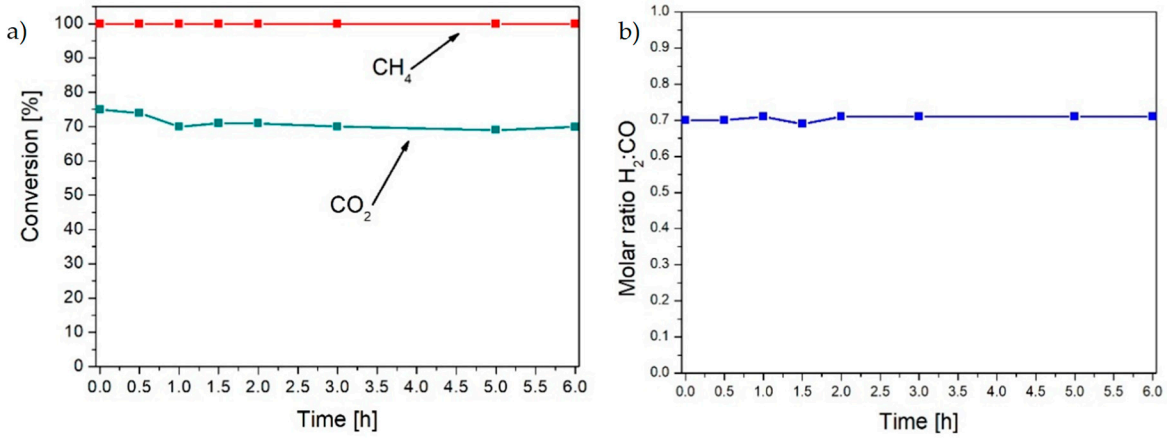

Figure 4. (**a**) Methane and carbon dioxide conversion and (**b**) hydrogen/carbon monoxide molar ratio for the 6 h test.

2.2.3. Carbon Deposits

Carbon deposits on the catalyst surface after the dry reforming process were quantified using CHNS elemental analysis. Table 2 presents the results of the measurements for selected catalysts. The carbon content is expressed in % by weight of the reactor bed.

Table 2. Carbon deposits content after the dry reforming process.

Catalyst	Carbon Content (wt.%)
$Ni/MgAl_2O_4$	<0.1
$Ru-Ni/MgAl_2O_4$	<0.1
Ni/SiO_2	0.38
$Ru-Ni/SiO_2$	0.42
Ni/Al_2O_3	<0.1
$Ru-Ni/Al_2O_3$	<0.1

The lowest contents were observed for catalysts showing the highest catalytic activity—$Ni/MgAl_2O_4$, $Ru-Ni/MgAl_2O_4$, Ni/Al_2O_3, and $Ru-Ni/Al_2O_3$. The carbon content was less than 0.1 wt.%. Carbon deposits were observed only for catalysts supported on silica—the carbon content was comparable to 0.38 wt.% and 0.42 wt.% for Ni/SiO_2 and $Ru-Ni/SiO_2$, respectively. The total carbon contents for Ni/SiO_2 and $Ru-Ni/SiO_2$ equaled 0.19 and 0.21 ug of carbon per 1 g of catalyst.

3. Discussion

The catalytic activity of nickel and ruthenium–nickel catalyst deposited on ZrO_2, Al_2O_3, $MgAl_2O_4$, and SiO_2 supports was investigated. The highest activity was observed for catalysts for both nickel and ruthenium–nickel catalysts supported on Al_2O_3 and $MgAl_2O_4$. The level of methane and carbon dioxide conversions for Ni/Al_2O_3 was constant through all catalytic process and equaled 95% and 85%, respectively. A similar effect in CO_2 conversion was observed for $Ni/MgAl_2O_4$, however, a lower level of methane conversion occurred. The hydrogen to carbon monoxide ratio for the most active samples was also the highest, close to unity, as is expected for dry reforming processes. Moreover, for most active samples, no carbon deposits were detected. The Ni/SiO_2 catalyst revealed the lowest activity and carbon deposition. The total carbon content equaled 0.19 $ug_C g_{cat}^{-1}$. No correlation between the BET surface area and catalytic activity was observed. The highest activity was observed for supports that

strongly interact with active metals. Based on the results of the hydrogen temperature-programmed reduction (H_2-TPR) that can be found in the literature for nickel particles supported on silica, it can be concluded that Ni particles weakly interact with SiO_2 [37,42], whereas with Al_2O_3 and $MgAl_2O_4$, nickel reduction temperatures are significantly higher, indicating strong interactions [9,42]. The high activity of catalysts supported on $MgAl_2O_4$ may also be a result of the basic features. Supports of the basic properties facilitate dissociative adsorption of CO_2 on the catalyst [1,9,43]. Park et al. [41] investigated the effect of supports on the catalytic activity of Co-Al catalysts during the dry reforming process. The catalytic activity decreased as follows: $CoAl/MgAl_2O_4 > CoAl/Al_2O_3 > CoAl/ZrO_2 > CoAl/CeO_2 > CoAl/SiO_2$. The differences in catalytic activity were attributed to the balance between the rate of carbon decomposition and surface oxidation, which are strictly dependent on the nature of the support. Han et al. [42] also investigated the effect of the support of catalysts during DRM reactions. They found that a high catalytic activity was a combined result of the nickel nanoparticle size, process temperature, and strong interactions of Ni with the support, especially with basic properties.

Further modification with ruthenium particles resulted in an increase in the methane conversion rate and product generation yield for catalysts obtained on silica supports and commercial aluminium (III) oxide. For $Ru\text{-}Ni/Al_2O_3$, almost all CH_4 was converted; even for the less active sample, $Ru\text{-}Ni/SiO_2$, the methane conversion increased to a level of around 65%. A decrease of the H_2:CO ratio for all ruthenium–nickel catalysts in comparison to catalysts containing only nickel particles was noted. For example, for the Ni/Al_2O_3 and $Ru\text{-}Ni/Al_2O_3$ sample, the H_2:CO ratio decreased from nearly 1.0 to 0.7, respectively, whereas for $Ni/MgAl_2O_4$, it decreased from about 0.9 to 0.65, respectively. According to the literature, noble metal particles, such as platinum, ruthenium, and rubidium, increase catalyst reducibility and resistance to carbon deposition by catalyzing the gasification reaction of carbon atoms, which results from carbon dioxide disproportionation, methane decomposition, and the carbon dioxide reaction with hydrogen (RWGS) [15]. The enhanced hydrogen generation as a result lowers the H_2:CO ratio, which may be caused by the additional promotion of methane dissociation observed in the presence of noble metal particles [44]. On the basis of X-ray diffraction crystallite size analysis (see Table 1), it was found that the average size of ruthenium(IV) oxide $Ru\text{-}Ni/SiO_2$ crystals was 8 nm, while for $Ru\text{-}Ni\text{-}MgAl_2O_4$, this was 32 nm. For $Ru\text{-}Ni/Al_2O_3$, no reflections were observed for RuO_2, which may indicate the presence of very small RuO_2 crystallites, resulting in an enhanced catalytic activity. According to the literature and the free energy values of Gibbs for dry reforming at 800 °C, the methane conversion rate can reach 95%, while carbon dioxide can reach 85% [7]. For ruthenium–nickel catalysts supported on $MgAl_2O_4$ and Al_2O_3, nearly maximum possible conversions were reached. Fluctuations in carbon dioxide and hydrogen can result from the occurrence of side reactions, including the oxide disproportionation reaction (called the Boudouard reaction) and the conversion of carbon(II) oxide with water vapor (RWGS) [10]. CHNS elemental analysis confirmed the effective gasification of carbon deposits for the most active catalysts. Carbon deposits were only detected only for $Ru\text{-}Ni/SiO_2$ at the amount of 0.21 $ug_c g_{cat}^{-1}$. For the $Ru/Ni\text{-}Al_2O_3$ catalyst, a 6 h test for stability during DRM conditions was performed. The catalyst exhibited high activity and stability. The methane and carbon dioxide conversions were constant throughout the whole process and equaled 98% to 100% and 75%, respectively. The H_2:CO ratio also remained at a constant level of 0.7.

4. Materials and Methods

4.1. Materials

Nickel nitrate hexahydrate 98%, ruthenium(III) chloride 99.9%, aluminium nitrate 98%, and magnesium nitrate 98% were purchased from Alfa Aesar, Kandel, Germany. Aluminium(III) oxide was obtained from Chempur, Piekary Śląskie, Poland. Tetraethyl orthosilicate, ethyl alcohol, and ammonia were purchased from POCH, Gliwice, Poland.

4.2. Catalyst Characterization

XRD analysis was performed using a Rigaku Intelligent X-ray diffraction system SmartLab equipped with a sealed tube X-ray generator (a copper target; operated at 40 kV and 30 mA), a D/teX high-speed position sensitive detector system, and an ASC-10 automatic sample changer. Data acquisition conditions were as follows: 2θ range: 5–90°, scan speed: 1° min^{-1} and scan step 0.008. Analysis of the crystal structure and planes, including Rietveld analysis, was performed using Rigaku PDXL software (Version 2.0, Rigaku Corporation, Neu-Isenburg, Germany, 2007).

The Brunauer, Emmett, and Teller (BET) surface analysis method was performed using the Micromeritics Gemini V apparatus (model 2365) (Norcross, GA, USA). Helium was used as the gas filling free spaces. The range of partial pressures, p/p_0, ranged from 0.05 to 0.3. Before the adsorption measurement, the samples were degassed at 473 K for two hours.

The final metal loading (wt.%) of the final catalysts was carried out using atomic emission spectroscopy with excitation in induced plasma (ICP-OES). The ICP-OES Agilent 5100 VDV (Santa Clara, CA, USA) apparatus with a Mars CEM sample mineralizer was used for the tests. Analysis of the elemental composition was preceded by the stage of mineralization of catalysts with nitric acid at 200 °C and pressure not exceeding 24 bar.

Carbon deposits on spent catalysts were evaluated using elemental analysis CHNS. The sample of the spent catalyst was encapsulated in tin foil and combusted in an excess of oxygen at 1060 °C. The amount of generated carbon dioxide was measured chromatographically using a Thermo Fisher Scientific Flash 2000 analyzer (Walthman, MA, USA) equipped with a thermal-conductivity detector. Nitrogen was used as the carrier gas. The limit od detection equaled 0.1 wt.%.

4.3. Catalyst Preparation

Monometallic and bimetallic nickel and ruthenium catalysts were obtained using impregnation and precipitation methods. Detailed descriptions of the preparation are presented in the subsections below.

4.3.1. Support Preparation

The magnesium–alumina spinel was obtained by chemical precipitation in a basic environment. Magnesium nitrate and aluminium nitrate were dissolved in deionized water and mixed to obtain a clear solution. The molar ratio of Mg:Al equaled 1:2. Subsequently, the pH was adjusted to pH 10 with ammonia. The resulting precipitate was subjected to 24 h of ageing at 50 °C. Then, the precipitated $MgAl_2O_4$ was separated, washed twice with deionized water, dried overnight at 100 °C, and calcinated at 400 °C for 6 h.

The preparation of silica was based on the Stöber method. First, SiO_2 was obtained via the hydrolysis of tetraethylorthosilicate (TEOS) in a basic environment. The hydrolysis was carried out by dropping a solution of tetraethylorthocoate in anhydrous ethyl alcohol into an aqueous solution of ammonia water. The amounts of reagents used were due to the stoichiometry of the reaction and our own preliminary research. The weight ratio of the reagents used for preparation equaled TEOS:H_2O:EtOH:NH_3 = 11:1.8:30:1. The sol obtained from the hydrolysis was aged at room temperature for 24 h. The resulting precipitate was then separated, washed with ethyl alcohol, water, dried overnight at 80 °C, and calcinated at 500 °C for 6 h. The temperature increase was maintained at 2 °C·min^{-1}.

Zirconium(IV) oxide was obtained by chemical precipitation in a basic environment. Zirconium(IV) nitrate was dissolved in deionized water at 40 °C. The resulting solution was then cooled to room temperature and alkalized with ammonia until the pH reached pH = 9. The obtained precipitate was separated, washed twice with water, and dried at 80 °C. The last stage was calcination at 600 °C for 5 h.

4.3.2. Preparation of Ni and Ni-Ru Catalysts

Nickel-based catalysts were obtained via impregnation of the support with metal ions followed by chemical precipitation. Previously prepared support, as described in Section 4.3.1, $MgAl_2O_4$, SiO_2, ZrO_2, or commercial Al_2O_3, after the drying step, was dispersed in deionized water. Then, solutions of metal salts (nickel(II) nitrate and/or ruthenium(III) chloride) were added dropwise and the pH was adjusted to 9. The precipitate was separated, washed twice with water, and dried at 80 °C. Obtained powders were calcinated at 400, 500, and 600 °C for Al_2O_3, $MgAl_2O_4$, SiO_2, and ZrO_2 supports [30,41,42], respectively. The metal content used for preparation was 7 wt.% and 1 wt.% for nickel and ruthenium, respectively.

4.4. Catalytic Activity

The catalytic activity of the obtained catalysts was investigated in a model reaction of the synthesis of carbon(II) oxide and hydrogen (synthesis gas). The tests were carried out in a tubular reactor with a length of 600 mm and an internal diameter of 4.5 mm. The catalytic bed consisted of catalyst in an amount of 5 wt.% diluted with quartz sand with a grain size in the range of 0.1 mm to 0.5 mm. A model mixture of substrates of carbon dioxide and methane were introduced into the reactor with a total flow rate of 400 cm^3 min^{-1} in a 1:1 volume ratio. The process temperature was maintained at 800 °C. The temperature inside the reactor was controlled throughout the process using a K120764 type thermocouple. The catalytic activity was expressed through the substrate conversion rate (CO_2 and CH_4) and product generation yield (H_2 and CO). The content of individual compounds in the mixture leaving the reactor was determined chromatographically using a Perkin Elmer Clarus 500 (Shelton, CT, USA) gas chromatograph equipped with a ShinCarbon ST100/120 (Restek Corporation, Bellefonte, PA, USA) packed column (length 1 m, internal diameter 1 mm) and a thermal-conductivity detector (TCD). Argon was used as the carrier gas.

Conversion levels and the molar ratio of hydrogen to carbon monoxide (II) were determined using the formulas shown below:

$$X_{CH_4}(\%) = \frac{n_{CH_4,in} - n_{CH_4,out}}{n_{CH_4,in}} \times 100,$$

$$X_{CO_2}(\%) = \frac{n_{CO_2,in} - n_{CO_2,out}}{n_{CO_2,in}} \times 100,$$

$$\text{Molar ratio} = \frac{n_{H_2,out}}{n_{CO,out}},$$

where $n_{i,in}$ and $n_{i,out}$ are the moles of each component in the feed or effluent, respectively.

5. Conclusions

In this work, we reported the effect of supports on the catalytic activity of nickel and ruthenium–nickel catalyst deposited on ZrO_2, Al_2O_3, $MgAl_2O_4$, and SiO_2. Unmodified supports did not reveal catalytic activity, which indicates the key role of nickel and ruthenium particles in the dry reforming process. The catalytic activity for nickel catalysts decreased in the following order: $Ni/Al_2O_3 > Ni/MgAl_2O_4 > Ni/ZrO_2 > Ni/SiO_2$, while for ruthenium–nickel catalysts, the same order was observed: $Ru\text{-}Ni/Al_2O_3 > Ru\text{-}Ni/MgAl_2O_4 > Ru\text{-}Ni/ZrO_2 > Ru\text{-}Ni/SiO_2$. The highest activity was observed for supports that strongly interact with nickel particles, which indicates the key role of support features on activity under DRM conditions. A comparison of substrate conversions and the H_2:CO product ratios for Ni and Ni–Ru catalysts revealed that the introduction of ruthenium particles to the process system results in the switching of the hydrogen to carbon monoxide ratio to lower values as a consequence of enhanced methane dissociation. Differences in the catalytic activities were probably a result of differences in the dispersion and particle size of active metals, as well as

interactions between support particles and active metals. Study on the effect of the particle size of nickel and ruthenium–nickel catalysts will be continued during further research.

Author Contributions: Conceptualization, methodology, writing; catalysts synthesis and characterization, I.W.; investigation, I.W., A.R.; review, J.H., A.R., editing, project administration, funding acquisition, A.R.

Funding: This research was cofounded by Polskie Górnictwo Naftowe i Gazownictwo PGNiG.

Acknowledgments: Authors highly acknowledge Justyna Łuczak from Gdańsk University of Technology for help during CHNS analysis.

Conflicts of Interest: The authors declare no conflict of interest.

References

1. Arora, S.; Prasad, R. An Overview on Dry Reforming of Methane: Strategies to Reduce Carbonaceous Deactivation of Catalysts. *RSC Adv.* **2016**, *6*, 108668–108688. [CrossRef]
2. Azizi, Z.; Rezaeimanesh, M.; Tohidian, T.; Rahimpour, M.R. Dimethyl Ether: A Review of Technologies and Production Challenges. *Chem. Eng. Process. Process Intensif.* **2014**, *82*, 150–172. [CrossRef]
3. Rostrup-Nielsen, J.R. Production of Synthesis Gas. *Catal. Today* **1993**, *18*, 305–324. [CrossRef]
4. Mortensen, P.M.; Dybkjær, I. Industrial Scale Experience on Steam Reforming of CO_2-Rich Gas. *Appl. Catal. A Gen.* **2015**, *495*, 141–151. [CrossRef]
5. Abdullah, B.; Abd Ghani, N.A.; Vo, D.V.N. Recent Advances in Dry Reforming of Methane over Ni-Based Catalysts. *J. Clean. Prod.* **2017**, *162*, 170–185. [CrossRef]
6. Luyben, W.L. Design and Control of the Dry Methane Reforming Process. *Ind. Eng. Chem. Res.* **2014**, *53*, 14423–14439. [CrossRef]
7. Chein, R.Y.; Chen, Y.C.; Yu, C.T.; Chung, J.N. Thermodynamic Analysis of Dry Reforming of CH_4 with CO_2 at High Pressures. *J. Nat. Gas Sci. Eng.* **2015**, *26*, 617–629. [CrossRef]
8. Abdulrasheed, A.; Jalil, A.A.; Gambo, Y.; Ibrahim, M.; Hambali, H.U.; Shahul Hamid, M.Y. A Review on Catalyst Development for Dry Reforming of Methane to Syngas: Recent Advances. *Renew. Sustain. Energy Rev.* **2019**, *108*, 175–193. [CrossRef]
9. Jang, W.J.; Shim, J.O.; Kim, H.M.; Yoo, S.Y.; Roh, H.S. A Review on Dry Reforming of Methane in Aspect of Catalytic Properties. *Catal. Today* **2018**, *324*, 15–26. [CrossRef]
10. Aramouni, N.A.K.; Touma, J.G.; Tarboush, B.A.; Zeaiter, J.; Ahmad, M.N. Catalyst Design for Dry Reforming of Methane: Analysis Review. *Renew. Sustain. Energy Rev.* **2018**, *82*, 2570–2585. [CrossRef]
11. Xu, Y.; Lin, Q.; Liu, B.; Jiang, F.; Xu, Y.; Liu, X. A Facile Fabrication of Supported Ni/SiO_2 Catalysts for Dry Reforming of Methane with Remarkably Enhanced Catalytic Performance. *Catalysts* **2019**, *9*, 183. [CrossRef]
12. Gangurde, L.S.; Sturm, G.S.J.; Valero-romero, M.J.; Mallada, R.; Santamaria, J.; Stankiewicz, A.; Stefanidis, G. Synthesis, Characterization, and Application of Ruthenium-Doped $SrTiO_3$ Perovskite Catalysts for Microwave-Assisted Methane Dry Reforming. *Chem. Eng. Process. Process. Intensif.* **2018**, *127*, 178–190. [CrossRef]
13. Zhou, H.; Zhang, T.; Sui, Z.; Zhu, Y.A.; Han, C.; Zhu, K.; Zhou, X. A Single Source Method to Generate Ru-Ni-MgO Catalysts for Methane Dry Reforming and the Kinetic Effect of Ru on Carbon Deposition and Gasification. *Appl. Catal. B Environ.* **2018**, *233*, 143–159. [CrossRef]
14. Jabbour, K.; El Hassan, N.; Casale, S.; Estephane, J.; El Zakhem, H. Promotional Effect of Ru on the Activity and Stability of Co/SBA-15 Catalysts in Dry Reforming of Methane. *Int. J. Hydrogen Energy* **2014**, *39*, 7780–7787. [CrossRef]
15. Li, D.; Nakagawa, Y.; Tomishige, K. Methane Reforming to Synthesis Gas over Ni Catalysts Modified with Noble Metals. *Appl. Catal. A Gen.* **2011**, *408*, 1–24. [CrossRef]
16. Dou, Y.; Pang, Y.; Gu, L.; Ding, Y.; Jiang, W.; Feng, X.; Ji, W.; Au, C.T. Core-Shell Structured Ru-Ni@SiO_2: Active for Partial Oxidation of Methane with Tunable H_2/CO Ratio. *J. Energy Chem.* **2018**, *27*, 883–889. [CrossRef]
17. Al-Fatesh, A.S.; Arafat, Y.; Atia, H.; Ibrahim, A.A.; Ha, Q.L.M.; Schneider, M.; M-Pohl, M.; Fakeeha, A.H. CO_2-Reforming of Methane to Produce Syngas over Co-Ni/SBA-15 Catalyst: Effect of Support Modifiers (Mg, La and Sc) on Catalytic Stability. *J. CO_2 Util.* **2017**, *21*, 395–404. [CrossRef]

18. Rouibah, K.; Barama, A.; Benrabaa, R.; Guerrero-caballero, J.; Kane, T. Dry Reforming of Methane on Nickel-Chrome, Nickel-Cobalt and Nickel-Manganese Catalysts. *Int. J. Hydrogen Energy* **2017**, *42*, 29725–29734. [CrossRef]
19. Yao, L.; Galvez, M.E.; Hu, C.; Da Costa, P. Synthesis Gas Production via Dry Reforming of Methane over Manganese Promoted Nickel/Cerium-Zirconium Oxide Catalyst. *Ind. Eng. Chem. Res.* **2018**, *57*, 16645–16656. [CrossRef]
20. Liu, H.; Hadjltaief, H.B.; Benzina, M.; Gálvez, M.E.; Da Costa, P. Natural Clay Based Nickel Catalysts for Dry Reforming of Methane: On the Effect of Support Promotion (La, Al, Mn). *Int. J. Hydrogen Energy* **2019**, *4*, 246–255. [CrossRef]
21. Das, S.; Ashok, J.; Bian, Z.; Dewangan, N.; Wai, M.H.; Du, Y.; Borgna, A.; Hidajat, K.; Kawi, S. Silica—Ceria Sandwiched Ni Core—Shell Catalyst for Low Temperature Dry Reforming of Biogas: Coke Resistance and Mechanistic Insights. *Appl. Catal. B Environ.* **2018**, *230*, 220–236. [CrossRef]
22. Kim, S.M.; Abdala, P.M.; Margossian, T.; Hosseini, D.; Foppa, L.; Armutlulu, A.; Van Beek, W.; Comas-Vives, A.; Copéret, C.; Müller, C. Cooperativity and Dynamics Increase the Performance of NiFe Dry Reforming Catalysts. *J. Am. Chem. Soc.* **2017**, *139*, 1937–1949. [CrossRef]
23. Margossian, T.; Larmier, K.; Kim, S.M.; Krumeich, F.; Müller, C.; Copéret, C. Supported Bimetallic NiFe Nanoparticles through Colloid Synthesis for Improved Dry Reforming Performance. *ACS Catal.* **2017**, *7*, 6942–6948. [CrossRef]
24. Świrk, K.; Gálvez, M.E.; Motak, M.; Grzybek, T.; Rønning, M.; Da Costa, P. Dry Reforming of Methane over Zr- and Y-Modified Ni/Mg/Al Double-Layered Hydroxides. *Catal. Commun.* **2018**, *117*, 26–32. [CrossRef]
25. Feng, X.; Liu, J.; Zhang, P.; Zhang, Q.; Xu, L.; Zhao, L.; Song, X.; Gao, L. Highly Coke Resistant Mg–Ni/Al_2O_3 Catalyst Prepared via a Novel Magnesiothermic Reduction for Methane Reforming Catalysis with CO_2: The Unique Role of Al–Ni Intermetallics. *Nanoscale* **2019**, *11*, 1262–1272. [CrossRef]
26. Nakhaei Pour, A.; Mousavi, M. Combined Reforming of Methane by Carbon Dioxide and Water: Particle Size Effect of Ni-Mg Nanoparticles. *Int. J. Hydrogen Energy* **2015**, *40*, 12985–12992. [CrossRef]
27. Nandini, A.; Pant, K.K.; Dhingra, S.C. K-, CeO_2-, and Mn-Promoted Ni/Al_2O_3 Catalysts for Stable CO_2 Reforming of Methane. *Appl. Catal. A Gen.* **2005**, *290*, 166–174. [CrossRef]
28. Bailey, K.M.; Campbell, T.K.; Falconer, J.L. Potassium Promotion of Ni/Al_2O_3 Catalysts. *Appl. Catal.* **1989**, *54*, 159–175.
29. Németh, M.; Srankó, D.; Károlyi, J.; Somodi, F.; Schay, Z.; Sáfrán, G.; Sajó, I.; Horváth, A. Na-Promoted Ni/ZrO_2 Dry Reforming Catalyst with High Efficiency: Details of Na_2O-ZrO_2-Ni Interaction Controlling Activity and Coke Formation. *Catal. Sci. Technol.* **2017**, *7*, 5386–5401. [CrossRef]
30. Wang, Y.; Yao, L.; Wang, Y.; Wang, S.; Zhao, Q.; Mao, D.; Hu, C. Low-Temperature Catalytic CO_2 Dry Reforming of Methane on Ni-Si/ZrO_2 Catalyst. *ACS Catal.* **2018**, *8*, 6495–6506. [CrossRef]
31. Galhenage, R.P.; Yan, H.; Tenney, S.A.; Park, N.; Henkelman, G.; Albrecht, P.; Mullins, D.R.; Chen, D.A. Understanding the Nucleation and Growth of Metals on TiO_2: Co Compared to Au, Ni, and Pt. *J. Phys. Chem. C* **2013**, *117*, 7191–7201. [CrossRef]
32. Zhang, R.; Xia, G.; Li, M.; Wu, Y.; Nie, H.; Li, D. Effect of Supports on the Performance of Ni-Based Catalysts in Methane Dry Reforming. *J. Fuel Chem. Technol.* **2015**, *43*, 1359–1365. [CrossRef]
33. Zhang, X.; Zhang, Q.; Tsubaki, N.; Tan, Y.; Han, Y. Carbon Dioxide Reforming of Methane over Ni Nanoparticles Incorporated into Mesoporous Amorphous ZrO_2 Matrix. *Fuel* **2015**, *147*, 243–252. [CrossRef]
34. Wang, F.; Xu, L.; Shi, W. Syngas Production from CO_2 Reforming with Methane over Core-Shell Ni@SiO_2 Catalysts. *J. CO_2 Util.* **2016**, *16*, 318–327. [CrossRef]
35. Ferreira-Aparicio, P.; Rodriguez-Ramos, I.; Anderson, J.A.; Guerrero-Ruiz, A. Mechanistic Aspects of the Dry Reforming of Methane over Ruthenium Catalysts. *Appl. Catal. A Gen.* **2000**, *202*, 183–196. [CrossRef]
36. Frontera, P.; Macario, A.; Aloise, A.; Antonucci, P.L.; Giordano, G.; Nagy, J.B. Effect of Support Surface on Methane Dry-Reforming Catalyst Preparation. *Catal. Today* **2013**, *218–219*, 18–29. [CrossRef]
37. Wang, F.; Han, B.; Zhang, L.; Xu, L.; Yu, H.; Shi, W. CO_2 Reforming with Methane over Small-Sized Ni@SiO_2 Catalysts with Unique Features of Sintering-Free and Low Carbon. *Appl. Catal. B Environ.* **2018**, *235*, 26–35. [CrossRef]
38. Habibi, N.; Wang, Y.; Arandiyan, H.; Rezaei, M. Effect of Substitution by Ni in $MgAl_2O_4$ Spinel for Biogas Dry Reforming. *Int. J. Hydrogen Energy* **2017**, *42*, 24159–24168. [CrossRef]

39. Zarei, M.; Meshkani, F.; Rezaei, M. Preparation of Mesoporous Nanocrystalline Ni-$MgAl_2O_4$ Catalysts by Sol-Gel Combustion Method and Its Applications in Dry Reforming Reaction. *Adv. Powder Technol.* **2016**, *27*, 1963–1970. [CrossRef]
40. Nazemi, M.K.; Sheibani, S.; Rashchi, F.; Gonzalez-Delacruz, V.M.; Caballero, A. Preparation of Nanostructured Nickel Aluminate Spinel Powder from Spent NiO/Al_2O_3 Catalyst by Mechano-Chemical Synthesis. *Adv. Powder Technol.* **2012**, *23*, 833–838. [CrossRef]
41. Park, J.; Yeo, S.; Chang, T. Effect of Supports on the Performance of Co-Based Catalysts in Methane Dry Reforming. *J. CO_2 Util.* **2018**, *26*, 465–475. [CrossRef]
42. Han, J.W.; Park, J.S.; Choi, M.S.; Lee, H. Uncoupling the Size and Support Effects of Ni Catalysts for Dry Reforming of Methane. *Appl. Catal. B Environ.* **2017**, *203*, 625–632. [CrossRef]
43. Lemonidou, A.A.; Vasalos, I.A. Carbon Dioxide Reforming of Methane Over. *Appl. Catal. A Gen.* **2002**, *228*, 227–235.
44. Pakhare, D.; Spivey, J. A Review of Dry (CO_2) Reforming of Methane over Noble Metal Catalysts. *Chem. Soc. Rev.* **2014**, *43*, 7813–7837. [CrossRef]